A Leaky Integrate-and-Fire Laser Neuron for Ultrafast Cognitive Computing

Mitchell A. Nahmias, *Student Member, IEEE*, Bhavin J. Shastri, *Member, IEEE*, Alexander N. Tait, *Student Member, IEEE*, and Paul R. Prucnal, *Fellow, IEEE*

***Abstract*—We propose an original design for a neuron-inspired photonic computational primitive for a large-scale, ultrafast cognitive computing platform. The laser exhibits excitability and behaves analogously to a leaky integrate-and-fire (LIF) neuron. This model is both fast and scalable, operating up to a billion times faster than a biological equivalent and is realizable in a compact, vertical-cavity surface-emitting laser (VCSEL). We show that—under a certain set of conditions—the rate equations governing a laser with an embedded saturable absorber reduces to the behavior of LIF neurons. We simulate the laser using realistic rate equations governing a VCSEL cavity, and show behavior representative of cortical spiking algorithms simulated in small circuits of excitable lasers. Pairing this technology with ultrafast, neural learning algorithms would open up a new domain of processing.**

***Index Terms*—Cognitive computing, excitability, leaky integrate-and-fire (LIF) neuron, mixed-signal, neural networks, neuromorphic, optoelectronics, photonic neuron, semiconductor lasers, spike processing, ultrafast, vertical-cavity surface-emitting lasers (VCSELs).**

I. Introduction

In an effort to break the limitations inherent in traditional von Neumann architectures, some recent projects in computing have sought more effective signal processing techniques by leveraging the underlying physics of devices [1]–[6]. Cognitive computing platforms inspired by biological neural networks could solve unconventional computing problems and outperform current technology in both power efficiency and complexity [7]–[9]. These novel systems rely on an alternative set of computational principles, including hybrid analog-digital signal representations, colocation of memory and processing, unsupervised learning, and distributed representations of information.

Manuscript received December 4, 2012; revised March 8, 2013; accepted April 3, 2013. Date of publication April 12, 2013; date of current version May 24, 2013. This work was supported in part by the Lockheed Martin Advanced Technology Laboratory through the IRAD program, in part by the Lockheed Martin Corporation through the Corporate University Research Program, and in part by the NSF MIRTHE Center at Princeton University, the Pyne Fund and Essig Enright Fund for Engineering in Neuroscience. The work of M. A. Nahmias and A. N. Tait was supported by the National Science Foundation Graduate Research Fellowship (NSF-GRF). The work of B. J. Shastri was supported by the National Sciences and Engineering Research Council of Canada (NSERC) Postdoctoral Fellowship (PDF).

The authors are with the Lightwave Communications Laboratory, Department of Electrical Engineering, Princeton University, Princeton, NJ 08544 USA (e-mail: mnahmias@princeton.edu; shastri@ieee.org; atait@Princeton.edu; prucnal@princeton.edu).

Color versions of one or more of the figures in this paper are available online at http://ieeexplore.ieee.org.

Digital Object Identifier 10.1109/JSTQE.2013.2257700

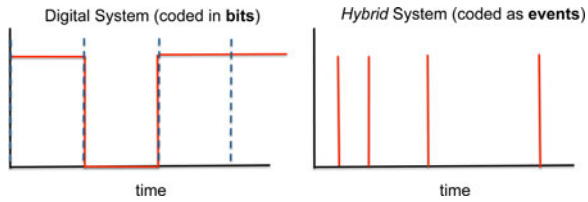

Fig. 1. Spiking neural networks encode information as events in time rather than bits. Because the time at which a spike occurs is analog while its amplitude is digital, the signals use a mixed signal or hybrid-encoding scheme.

On the cellular level, the brain encodes information as events or *spikes* in time [10], a hybrid signal with both analog and digital properties as illustrated in Fig. 1. This encoding scheme is equivalent to analog *pulse position modulation* (PPM) in optics, which has been utilized in various applications including the implementation of robust chaotic communication [11] and power efficient channel coding [12]. Spike processing has evolved in biological (nervous systems) and engineered (neuromorphic analog VLSI) systems as a means to exploit the efficiency of analog signals while overcoming the problem of noise accumulation inherent in analog computation [13]. Various technologies have emulated spike neural networks in electronics, including IBM's neurosynaptic core as part of DARPA's SyNAPSE program [1], [2] and Neurogrid as part of Stanford's Brains in Silicon program [14]. Although these architectures have garnered success in various applications, they aim to target biological time scales rather than exceed them. Microelectronic neural networks that are both fast and highly interconnected are subject to a fundamental bandwidth fan-in tradeoff.

Photonic platforms offer an alternative approach to microelectronics. The high speeds, high bandwidth, and low crosstalk achievable in photonics are very well suited for an ultrafast spike-based information scheme. Because of this, photonic spike processors could access a computational domain that is inaccessible by other technologies. This domain, which we describe as *ultrafast cognitive computing*, represents an unexplored processing paradigm that could have a wide range of applications in adaptive control, learning, perception, motion control, sensory processing (vision systems, auditory processors, and the olfactory system), autonomous robotics, and cognitive processing of the radio frequency spectrum.

There has been a growing interest in photonic spike processing which has spawned a rich search for an appropriate computational primitive. The first category includes those based on discrete, fiber components [15]–[17]. However, the platform's reliance on nonlinear fibers and other similar technologies have made demonstrations bulky (on the order of meters), complex,

and power-hungry (hundreds of watts). The platform is simply unscalable beyond a few neurons. Integrated lasers, in contrast, are physically compact and are capable of using feedback rather than feedforward dynamics to radically enhance nonlinearity. Feedback allows for the emergence of more complex behaviors, including bistability, the formation of attractors, and excitability.

Excitability is a dynamical system property that underlies all-or-none responses. Its occurrence in a variety of different lasing systems has received considerable interest [18], [19]. Excitability is also a critical property of biological spiking neurons [20], [21]. More recently, several excitable lasers have demonstrated biological-like spiking features. One proposal suggests using excitability in semiconductor lasers [22], [23] based on weakly broken $\mathbb{Z}_2$ symmetry close to a Takens–Bogdanov bifurcation, yet another suggests using emergent biological features from polarization switching in a vertical-cavity surface-emitting laser (VCSEL) [24]. However, these models have yet to demonstrate some key properties of spiking neurons: the ability to perform computations without information degradation, clean-up noise, or implement algorithms.

In this paper, we show for the first time that a photonic computational primitive based on an integrated, excitable laser with an embedded saturable absorber (SA) behaves analogously to a leaky integrate-and-fire (LIF) neuron. The LIF model is one of the most ubiquitous models in computational neuroscience and is the simplest known model for spike processing [25]. We also show that our laser neuron can be employed to carry out cortical algorithms through several small circuit demonstrations. Emulating this model in a scalable device represents the first step in building an ultrafast cognitive computing platform.

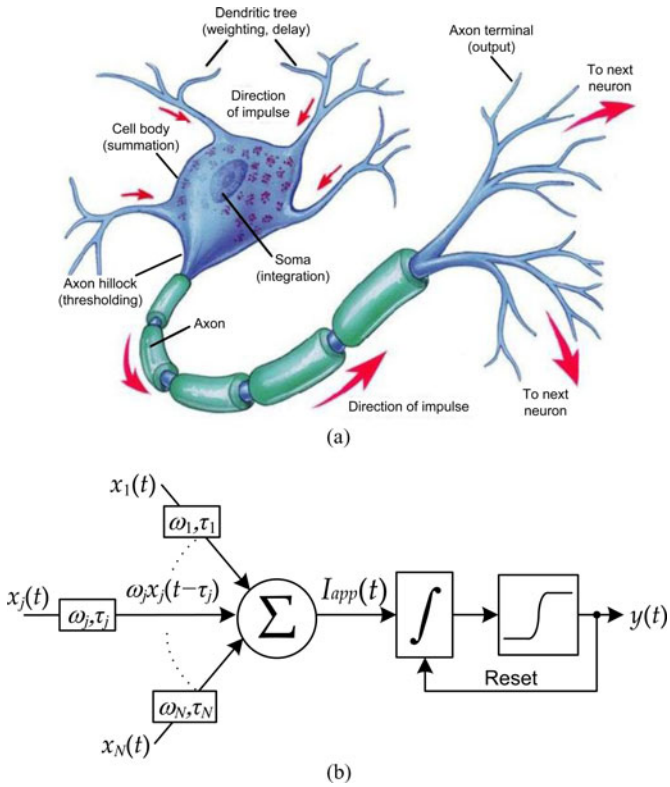

Fig. 2. (a) Illustration and (b) functional description of a leaky integrate-and-fire neuron. Weighted and delayed input signals are summed into the input current $I_{\mathrm{app}}(t)$, which travel to the soma and perturb the internal state variable, the voltage V. Since V is hysteric, the soma performs integration and then applies a threshold to make a spike or no-spike decision. After a spike is released, the voltage V is reset to a value V_{reset}. The resulting spike is sent to other neurons in the network.

II. Laser Neuron—Theoretical Foundations

Our device is based upon a well-studied and paradigmatic example of a hybrid computational primitive: the spiking neuron. In this section, we briefly review the spiking neuron model and reveal the analogy between the LIF model and our own.

A. Spiking Neuron Model

Studies of morphology and physiology have pinpointed the LIF model as an effective spiking model to describe a variety of different biologically observed phenomena [26]. From the standpoint of computability and complexity theory, LIF neurons are powerful computational primitives that are capable of simulating both Turing machines and traditional sigmoidal neural networks [27]. Signals are ideally represented by series of delta functions: inputs and outputs take the form $x(t) = \Sigma_{j=1}^{n} \delta(t - \tau_j)$ for spike times τ_j. Individual units perform a small set of basic operations (delaying, weighting, spatial summation, temporal integration, and thresholding) that are integrated into a single device capable of implementing a variety of processing tasks, including binary classification, adaptive feedback, and temporal logic.

The basic biological structure of an LIF neuron is depicted in Fig. 2(a). It consists of a dendritic tree that collects and sums inputs from other neurons, a soma that acts as a low-pass filter and integrates the signals over time, and an axon that carries an action potential, or spike, when the integrated signal exceeds a threshold. Neurons are connected to each other via synapses, or extracellular gaps, across which chemical signals are transmitted. The axon, dendrite, and synapse all play an important role in the weighting and delaying of spike signals.

According to the standard LIF model, neurons are treated as electrical devices. The membrane potential $V_m(t)$, the voltage difference across their membrane, acts as the primary internal (activation) state variable. Ions that flow across the membrane experience a resistance $R = R_m$ and capacitance $C = C_m$ associated with the membrane. The soma is effectively a first-order low-pass filter, or a leaky integrator, with the integration time constant $\tau_m = R_m C_m$ that determines the exponential decay rate of the impulse response function. The leakage current through R_m drives the membrane voltage $V_m(t)$ to 0, but an active membrane pumping current counteracts it and maintains a resting membrane voltage at a value of $V_m(t) = V_L$.

Fig. 2(b) shows the standard LIF neuron model [27]. A neuron has: 1) N inputs which represent induced currents in input synapses $x_j(t)$ that are continuous time series consisting either of spikes or continuous analog values; 2) an internal activation state $V_m(t)$; and 3) a single output state $y(t)$. Each input is independently weighted by ω_j, which can be positive or negative, and delayed by τ_j resulting in a time series that is spatially summed (summed pointwise). This aggregate input induces an

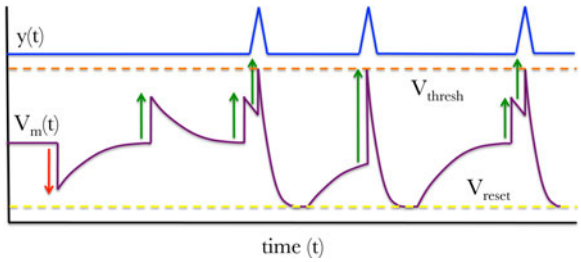

Fig. 3. An illustration of spiking dynamics in an LIF neuron. Spikes arriving from inputs $x_j(t)$ that are inhibitory (red arrows) reduce the voltage $V(t)$, while those that are excitatory (green arrows) increase $V(t)$. Enough excitatory activity pushes $V(t)$ above V_{thresh}, releasing a delta function spike in $y(t)$, followed by a refractory period during which $V(t)$ recovers to its resting potential V_L.

electrical current, $I_{\text{app}}(t) = \Sigma_{j=1}^{n} \omega_j x_j(t - \tau_j)$ between adjacent neurons.

The weights w_j and delays τ_j determine the dynamics of network, providing a way of programming a neuromorphic system. The parameters internal to the behavior of individual neurons include the resting potential V_L and the membrane time constant τ_m. There are three influences on $V_m(t)$—passive leakage of current, an active pumping current, and external inputs generating time-varying membrane conductance changes. Including a set of digital conditions, we arrive at a typical LIF model for an individual neuron:

$$\underbrace{\frac{dV_m(t)}{dt}}_{\text{Activation}} = \underbrace{\frac{V_L}{\tau_m}}_{\text{Active pumping}} - \underbrace{\frac{V_m(t)}{\tau_m}}_{\text{Leakage}} + \underbrace{\frac{1}{C_m} I_{\text{app}}(t)}_{\text{External input}}; \quad \text{(1a)}$$

$$\text{if } V_m(t) > V_{\text{thresh}}, \text{ then}$$

$$\text{release a pulse at } t_f \text{ and set } V_m(t) \rightarrow V_{\text{reset}}. \quad \text{(1b)}$$

The dynamics of an LIF neuron are illustrated in Fig. 3. If $V_m(t) \geq V_{\text{thresh}}$, then the neuron outputs a spike which takes the form $y(t) = \delta(t - t_f)$, where t_f is the time of spike firing, and $V_m(t)$ is set to V_{reset}. This is followed by a *relatively refractory period*, during which $V_m(t)$ recovers from V_{reset} to the resting potential V_L in which is difficult, but possible to induce the firing of a spike. [1] Consequently, the output of the neuron consists of a continuous time series comprised of spikes taking the form $y(t) = \Sigma_i \delta(t - t_i)$ for spike firing times t_i.

B. Excitable Laser Model

Our starting point is a set of dimensionless equations describing SA lasers that can generalize to a variety of different systems, including passively Q-switched microchip lasers [28], distributed Bragg reflector lasers [29], and VCSELs [30]. Below, we will show that a series of approximations leads to behavior that is isomorphic with LIF neurons.

[1]There may also be a short, *absolute refractory period* τ_{refrac} for which $V_m(t_f + \Delta t) = V_{\text{reset}}$ if $\Delta t \leq \tau_{\text{refrac}}$, and during which no spikes may be fired. Although this condition typically precedes the relative refractory period, we have omitted this from the model since it does not significantly affect the underlying dynamics.

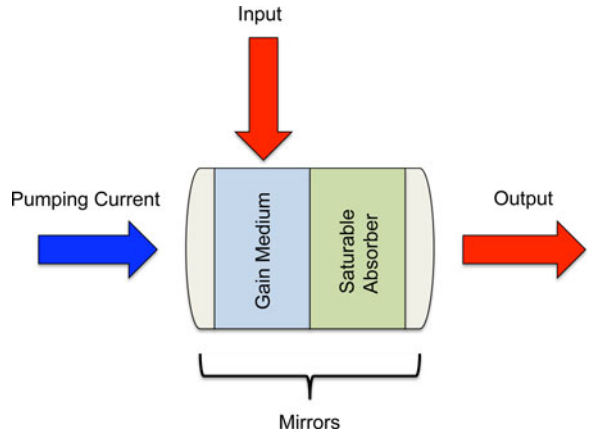

Fig. 4. A simple schematic of an SA laser. The device is composed of (i) a gain section, (ii) a saturable absorber, and (iii) mirrors for cavity feedback. In the LIF excitable model inputs selectively perturb the gain optically or electrically.

We begin with the Yamada model [31], which describe the behavior of lasers with independent gain and SA sections with an approximately constant intensity profile across the cavity as illustrated in Fig. 4. We assume that the SA has a very short relaxation time on the order of the cavity intensity, which can be implemented either through doping or special material properties. The dynamics now operate such that the gain is a slow variable, while the intensity and loss are both fast. This 3-D dynamical system can be described with the following equations:

$$\dot{G}(t) = \gamma_G \left[A - G(t) - G(t)I(t)\right] \quad \text{(2a)}$$

$$\dot{Q}(t) = \gamma_Q \left[B - Q(t) - aQ(t)I(t)\right] \quad \text{(2b)}$$

$$\dot{I}(t) = \gamma_I \left[G(t) - Q(t) - 1\right] I(t) + \epsilon f(G) \quad \text{(2c)}$$

where $G(t)$ models the gain, $Q(t)$ is the absorption, $I(t)$ is the laser intensity, A is the bias current of the gain, B is the level of absorption, a describes the differential absorption relative to the differential gain, γ_G is the relaxation rate of the gain, γ_Q is the relaxation rate of the absorber, γ_I is the reverse photon lifetime, and $\epsilon f(G)$ represents the small contributions to the intensity made by spontaneous emission, (noise term) where ϵ is very small.[2]

We further assume that inputs to the system cause perturbations to the gain $G(t)$ only. Pulses—from other excitable lasers, for example—will induce a change $\triangle G$ as illustrated by the arrows in Fig. 5 and analog inputs will modulate $G(t)$ continuously. This can be achieved either injection via the optical pulses that selectively modulate the gain medium or through electrical current injection. We also make the additional assumption that the laser exhibits behavior similar to region 2 of the bifurcation diagram presented in [31], but with a fast absorber.

1) Before Pulse Formation: Since the loss $Q(t)$ and the intensity $I(t)$ are fast, they will quickly settle to their equilibrium values. On slower time scales, our system behaves as:

$$\dot{G}(t) = \gamma_G \left[A - G(t) - G(t)I(t)\right] + \theta(t) \quad \text{(3a)}$$

[2]Nondimensionalization allows us to set γ_I to 1, but we include this variable in our description to explicitly compare time scales between variables G, Q, and I.

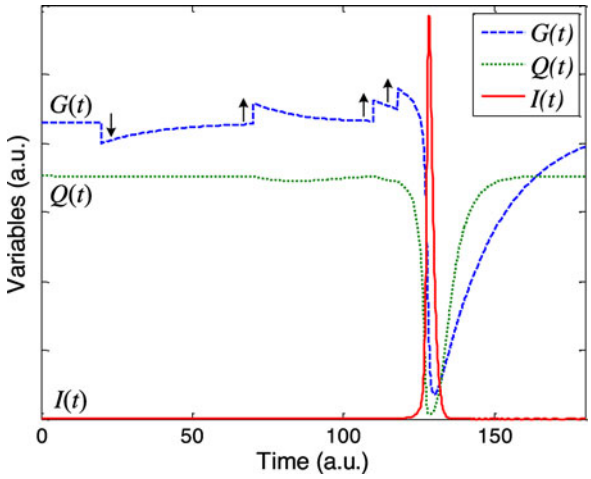

Fig. 5. Simulation results of an SA laser behaving as an LIF neuron. Arrows indicate excitatory pulses and inhibitory pulses that change the gain by some amount $\triangle G$. Enough excitatory input causes the system to enter fast dynamics in which a spike is generated, followed by the fast recover of the absorption $Q(t)$ and the slow recover of the gain $G(t)$. Variables were rescaled to fit within the desired range. Values used: $A = 4.3; B = 3.52; a = 1.8; \gamma_G = .05; \gamma_L, \gamma_I \gg .05$.

$$Q(t) = Q_{\text{eq}} \tag{3b}$$

$$I(t) = I_{\text{eq}} \tag{3c}$$

with $\theta(t)$ representing possible inputs, and the equilibrium values $Q_{\text{eq}} = B$ and $I_{\text{eq}} = \epsilon f(G)/\gamma_I \left[1 - G(t) + Q(t)\right]$. Since ϵ is quite small, $I_{\text{eq}} \approx 0$. With zero intensity in the cavity, the $G(t)$ and $Q(t)$ variables are dynamically decoupled. The result is that if inputs are incident on the gain, they will only perturb $G(t)$ unless $I(t)$ becomes sufficiently large to couple the dynamics together.

If $I(t)$ increases, the slow dynamics will break. Since $\dot{I}(t) \approx \gamma_I \left[G(t) - Q(t) - 1\right] I(t), I(t)$ will reach instability when $G(t) - Q(t) - 1 > 0$. Given our perturbations to $G(t)$, we can define a threshold condition:

$$G_{\text{thresh}} = Q + 1 = B + 1 \text{ (at equilibrium)} \tag{4}$$

above which fast dynamics will take effect. This occurs after the third excitatory pulse in Fig. 5.

2) Pulse Generation: Perturbations that cause $G(t) > G_{\text{thresh}}$ will result in the release of a short pulse. Once $I(t)$ is lifted above the invariant plane $\{I = 0\}, I(t)$ will increase exponentially. This results in the saturation of $Q(t)$ and the depletion of the gain $G(t)$. Once $G(t) - Q(t) - 1 < 0, I(t)$ will hit its peak intensity $I_{\max}$ and $Q(t)$ will reach its minimum $Q \approx 0$, followed by a fast decay of both I and Q on the order of $1/\gamma_I$ and $1/\gamma_Q$ in time, respectively. $I(t)$ will eventually reach $I \approx 0$ as it further depletes the gain to a final value G_{reset}, which—with a large enough intensity—is often close to the transparency level, i.e., $G_{\text{reset}} \approx 0$.

A given pulse derives its energy from excited carriers in the cavity. The total energy of the pulse is $E_{\text{pulse}} = N h\nu$, where N is the number of excited carriers that have been depleted and $h\nu$ is the energy of a single photon at the lasing frequency. Because the gain is proportional to the inversion population, N must

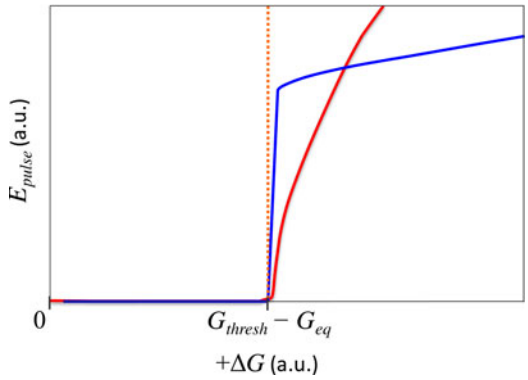

Fig. 6. Normalized, simulated transfer functions for a single pulse, operating the laser with a low equilibrium state (red curve) and a near-threshold equilibrium (blue curve). When a perturbation $\triangle G$ brings $G(t)$ above G_{thresh} (i.e. $\triangle G = G_{\text{thresh}} - G_{\text{eq}}$), the neuron fires a pulse with energy E_{pulse}. Setting G_{eq} close to G_{thresh} reduces the required perturbation $\triangle G$ to initiate a pulse and thereby minimizes the impact it has on the resulting output pulse, leading to the flatter region above threshold on the blue curve. A laser operating near threshold would minimize amplitude variations in the output.

be proportional to the amount that the gain $G(t)$ has depleted during the formation of a pulse. Thus, if G_{fire} is the gain that causes the release of a pulse, we can expect that an output pulse will take the approximate form:

$$P_{\text{out}} = E_{\text{pulse}} \cdot \delta(t - \tau_f) \tag{5}$$

$$E_{\text{pulse}} \propto G_{\text{fire}} - G_{\text{reset}} \tag{6}$$

where τ_f is the time at which a pulse is triggered to fire and $\delta(t)$ is a delta function. One of the properties of spike-encoded channels is that spike energies are encoded digitally. Spikes must have a constant amplitude every iteration, a characteristic property of the *all-or-nothing* response shared by biological neurons. We can normalize our output pulses if we set our system to operate close to threshold $G_{\text{thresh}} - G_{\text{eq}} \ll G_{\text{thresh}}$. Since the threshold is effectively lowered, the size of input perturbations $\triangle G$ must be scaled smaller. This implies $G_{\text{fire}} \approx G_{\text{thresh}}$, which helps in suppressing variations in the output pulse amplitude by reducing the input perturbation to the system. This leads to a step-function like response, as illustrated in Fig. 6, which is the desired behavior.

After a pulse is released, $I(t) \to 0$ and $Q(t)$ will quickly recover to Q_{eq}. The fast dynamics will give way to slower dynamics, in which $G(t)$ will slowly creep from G_{reset} to G_{eq}. The fast dynamics of $Q(t)$ assure that the threshold $G_{\text{thresh}} = 1 + Q(t)$ recovers quickly after a pulse is generated, preventing partial pulse release during the recovery period. In addition, the laser will experience a *relative refractory period* in which it is difficult—but not impossible—to fire another pulse.

3) LIF Analogy: If we assume the fast dynamics are nearly instantaneous, then we can compress the behavior of our system into the following set of equations and conditions:

$$\frac{dG(t)}{dt} = -\gamma_G \left(G(t) - A\right) + \theta(t); \tag{7a}$$

$$\text{if } G(t) > G_{\text{thresh}}, \text{ then}$$

$$\text{release a pulse, and set } G(t) \to G_{\text{reset}}. \tag{7b}$$

where $\theta(t)$ represent input perturbations. This behavior can be seen qualitatively in Fig. 5. The conditional statements account for the fast dynamics of the system that occur on times scales of order $1/\gamma_I$, and other various assumptions—including the fast $Q(t)$ variable and operation close to threshold—assure that $G_{\rm thresh}, G_{\rm reset}$ and the pulse amplitude $E_{\rm pulse}$ remain constant. If we compare this to the LIF model, or equation (1):

$$C_m \frac{dV_m(t)}{dt} = -\frac{1}{R_m}(V_m(t) - V_L) + I_{\rm app}(t);$$
$$\text{if } V_m(t) > V_{\rm thresh}, \text{ then}$$
$$\text{release a spike and set } V_m(t) \rightarrow V_{\rm reset}.$$

The analogy between the equations becomes clear. Setting the variables $\gamma_G = 1/R_m C_m, A = V_L, \theta(t) = I_{\rm app}(t)/R_m C_m$, and $G(t) = V_m(t)$ shows their algebraic equivalence. Thus, the gain of the laser $G(t)$ can be thought of as a virtual *membrane voltage*, the input current A as a virtual *leakage voltage*, etc.[3] There is a key difference; however—both dynamical systems operate on vastly different time scales. Whereas biological neurons have time constants $\tau_m = C_m R_m$ on order of milliseconds, carrier lifetimes of laser gain sections are typically in the nanosecond range and can go down to picosecond.

III. Excitable VCSELs

Although the excitable model is generalizable to a variety of different laser types, VCSELs are a particularly attractive candidate for our computational primitive as they occupy small footprints, can be fabricated in large arrays allowing for massive scalability, and use low powers [32]. An excitable, VCSEL with an intracavity SA that operates using the same rate equation model described previously has already been experimentally realized [33]. In addition, the technology is amenable to a variety of different interconnect schemes: VCSELs can send signals upward and form 3-D interconnects [34], can emit downward into an interconnection layer via grating couplers [35] or connect monolithically through intracavity holographic gratings [36].

A schematic of our VCSEL structure, which includes an intracavity SA, is illustrated in Fig. 7. To simulate the device, we use a typical two-section rate equation model such as the one described in [30]:

$$\frac{dN_{\rm ph}}{dt} = \Gamma_a g_a (n_a - n_{0a}) N_{\rm ph} + \Gamma_s g_s (n_s - n_{0s}) N_{\rm ph} - \frac{N_{\rm ph}}{\tau_{\rm ph}} + V_a \beta B_r n_a^2 \tag{8a}$$

$$\frac{dn_a}{dt} = -\Gamma_a g_a (n_a - n_{0a}) \frac{(N_{\rm ph} - \phi(t))}{V_a} - \frac{n_a}{\tau_a} + \frac{I_a + i_e(t)}{eV_a} \tag{8b}$$

$$\frac{dn_s}{dt} = -\Gamma_s g_s (n_s - n_{0s}) \frac{N_{\rm ph}}{V_s} - \frac{n_s}{\tau_s} + \frac{I_s}{eV_s} \tag{8c}$$

[3]Our laser lacks an *absolute refractory period* variable $\tau_{\rm refrac}$ seen in some LIF models, but the absence of this condition does not significantly affect its qualitative behavior.

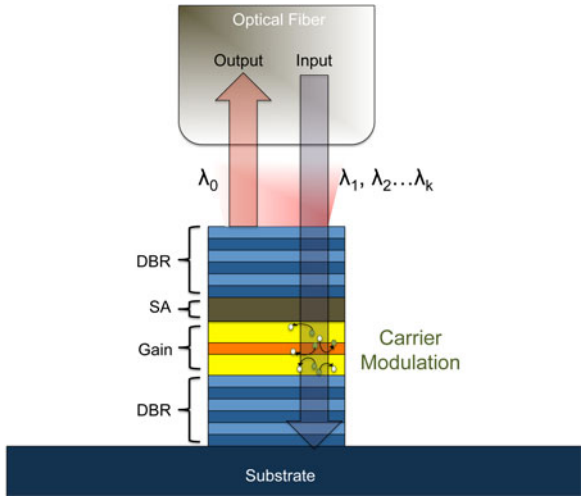

Fig. 7. A schematic diagram of a VCSEL-SA embedded in a network. In this configuration, inputs $\lambda_1, \lambda_2, \ldots, \lambda_n$ modulate the gain selectively. Various frequencies lie on different parts of the gain spectrum, leading to different excitatory and inhibitory responses. The weights and delays are applied by amplifiers and delay lines within the fiber network. If excited, a pulse at wavelength λ_0 is emitted upward and is eventually incident on other excitable lasers.

TABLE I
VCSEL-SA Excitable Laser Parameters [37]–[40]

Param.	Description	Value
λ	Lasing wavelength	850 nm
V_a	gain region cavity volume	2.4×10^{-18} m^3
V_s	SA region cavity volume	2.4×10^{-18} m^3
Γ_a	gain region confinement factor	0.06
Γ_s	SA region confinement factor	0.05
τ_a	gain region carrier lifetime	1 ns
τ_s	SA region carrier lifetime	100 ps
τ_p	Photon lifetime	4.8 ps
g_a	gain region differential gain/loss	2.9×10^{-12} m^{3}s^{-1}
g_s	SA region differential gain/loss	14.5×10^{-12} m^{3}s^{-1}
n_{0a}	gain region transparency carrier density	1.1×10^{24} m^{-3}
n_{0s}	SA region transparency carrier density	0.89×10^{24} m^{-3}
B_r	Bimolecular recombination term	10×10^{-16} m^{3}s^{-1}
β	Spontaneous emission coupling factor	1×10^{-4}
η_c	Output power coupling coefficient	0.4

where $N_{\rm ph}(t)$ is the total number of photons in the cavity, $n_a(t)$ is the number of carriers in the gain region, and $n_s(t)$ is the number of carriers in the absorber. Subscripts a and s identify the active and absorber regions, respectively. The remaining device parameters are summarized in Table I. We add an additional input term $\phi(t)$ to account for optical inputs selectively coupled into the gain, an additional modulation term $i_e(t)$ to represent electrical modulation in the gain, and an SA current injection term I_s/eV_s to allow for an adjustable threshold. For small perturbations, $\phi(t)$ and $i_e(t)$ possess similar functionalities and represent equally valid ways of modulating our laser with analog inputs.

These equations are analogous to the dimensionless set of equations (2) provided that the following coordinate

transformations are made:

$$G(\tilde{t}) = \tau_{\rm ph}\Gamma_a g_a(n_a(t) - n_{0a}), \quad I(\tilde{t}) = \frac{\tau_a\Gamma_a g_a}{V_a}N_{\rm ph}(t)$$

$$Q(\tilde{t}) = \tau_{\rm ph}\Gamma_s g_s(n_{0s} - n_s(t)), \quad \tilde{t} = \frac{t}{\tau_{\rm ph}}$$

where differentiation is now with respect to $\tilde{t}$ rather than t. The dimensionless parameters are now

$$\gamma_G = \frac{\tau_{\rm ph}}{\tau_a}, \quad A = \tau_a\tau_{\rm ph}\Gamma_a g_a\left[\frac{I_a}{eV_a} - \frac{n_{0a}}{\tau_a}\right]$$

$$\gamma_Q = \frac{\tau_{\rm ph}}{\tau_s}, \quad B = \tau_s\tau_{\rm ph}\Gamma_s g_s\left[\frac{n_{0s}}{\tau_s} - \frac{I_s}{eV_s}\right]$$

$$\gamma_I = 1, \quad a = \frac{\tau_s\Gamma_s g_s V_a}{\tau_a\Gamma_a g_a V_s}$$

$$\epsilon f(G) = \tau_a\tau_{\rm ph}\Gamma_a g_a\beta B_r n_a^2.$$

For the simulation, we set the input currents to $I_a = 2$ mA and $I_s = 0$ mA for the gain and absorber regions, respectively. The output power is proportional to the photon number $N_{\rm ph}$ inside the cavity via the following formula:

$$P_{\rm out}(t) \approx \frac{\eta_c\Gamma_a}{\tau_p}\frac{hc}{\lambda}N_{\rm ph}(t) \tag{9}$$

in which η_c is the output power coupling coefficient, c the speed of light, and hc/λ is the energy of a single photon at wavelength λ. We assume the structure is grown on a typical GaAs-based substrate and emits at a wavelength of 850 nm.

Using the parameters described previously, we simulated the device with optical injection into the gain as shown in Fig. 8. Input perturbations that cause gain depletion or enhancement—represented by positive and negative input pulses—modulate the carrier concentration inside the gain section. Enough excitation eventually causes the laser to enter fast dynamics and fire a pulse. This behavior matches an LIF neuron model as described in Section II-B3.

Our simulation effectively shows that an excitable LIF neuron is physically realizable in a VCSEL-SA cavity structure. The carrier lifetime of the gain is on the order of 1 ns, which as we have shown in Section II-B3 is analogous to the $R_m C_m$ time constant of a biological neuron—typically on the order of 10 ms. Thus, our device already exhibits speeds that are 10 million times faster than a biological equivalent. Lifetimes could go as short as a picosecond, making the potential factor speed increase between biology and photonics up to a billion.

IV. Cortical Spike Algorithms—Small-Circuit Demonstrations

Since our laser behaves identically to an LIF model, we can create a wide variety of useful networks that can implement a diversity of cortical functions. This section describes implementation of biologically inspired circuits with the excitable laser computational primitive. We have constructed circuits with unique properties as a proof of concept of system creation and wireability. These examples form a basis for a small-scale validity of any theoretical or experimental demonstration of important processing tasks that underlie many spiking neural networks. Though rudimentary, the circuits presented here are fundamental exemplars of three spike processing functions: multistable operation, synfire processing [41], and spatiotemporal pattern recognition [42]. Multistability forms the basis of attractor networks [43], synfire chains describe a mechanism with which neurons can form distributed representations of information to avoid noise degradation [44], and pattern recognition has been implicated in playing a crucial component in working memory [45].

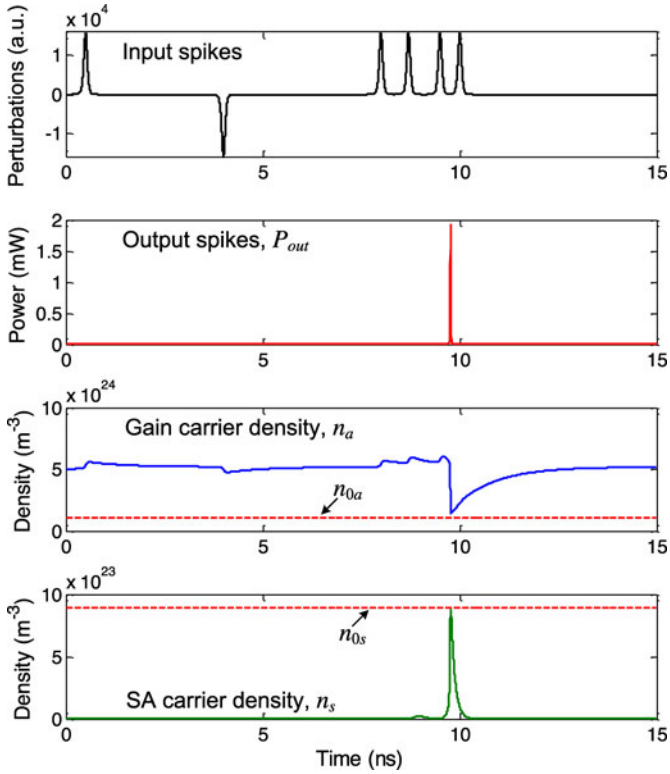

Fig. 8. Simulation of an excitable, LIF VCSEL-SA with realistic parameters. Inputs (top) selectively modulate the carrier concentration in the gain section (middle). Enough excitation leads to the saturation of the absorber to transparency (bottom) and the release of a pulse, followed by a relative refractory period while the pump current recovers the carrier concentration back to its equilibrium value.

We stipulate a mechanism for optical outputs of excitable lasers to selectively modulate the gain of others through both excitatory (gain enhancement) and inhibitory (gain depletion) pulses as illustrated in Fig. 7. Selective coupling into the gain can be achieved by positioning the gain and saturable absorber regions to interact only with specific optical frequencies as experimentally demonstrated in [33]. Excitation and inhibition can be achieved via the gain section's frequency dependent absorption spectrum—different frequencies can induce gain enhancement or depletion. This phenomenon has been experimentally demonstrated in semiconductor optical amplifiers (SOAs) [46] and could generalize to laser gain sections if the cavity modes are accounted for. Alternatives to these proposed solutions include photodetectors with short electrical connections and injection into an extended gain region in which excited carriers are swept into the cavity via carrier transport mechanisms.

A network of excitable lasers connected via weights and delays—consistent with the model described in Section II-A—can be described as a delayed differential equation (DDE) of the form:

$$\frac{d}{dt}\vec{x}(t) = f(\vec{x}(t), \vec{x}(t-\tau_1), \vec{x}(t-\tau_2)\ldots\vec{x}(t-\tau_n)) \quad (10)$$

where the vector $\vec{x}(t)$ contains all the state variable associated with the system. The output to our system is simply the output power $\vec{P_{\text{out}}}(t)$,[4] while the input is a set of weighted and delayed outputs from the network $\sigma(t) = \sum_k W_k \vec{P}_{\text{out}}(t-\tau_k)$. We can construct weight and delay matrices W, D such that the W_{ij} element of W represents the strength of the connection between excitable lasers i, j, and the D_{ij} element of D represents the delay between lasers i, j. If we recast (8) in a vector form, we can formulate our system in (10) given that the input function vector $\vec{\phi}(t)$ is

$$\vec{\phi}(t) = \Omega\vec{\Theta}(t) \quad (11)$$

where we create a sparse matrix Ω containing information for both W and D, and a vector $\vec{\Theta}(t)$ that contains all the past outputs from the system during unique delays $U = [\tau_1, \tau_2, \tau_3, \ldots, \tau_n]$:

$$\Omega = [W_0\ W_1\ W_2 \ldots W_n] \quad (12)$$

$$\vec{\Theta}(t) = \begin{pmatrix} \vec{P_{\text{out}}}(t) \\ \vec{P_{\text{out}}}(t-\tau_1) \\ \vec{P_{\text{out}}}(t-\tau_2) \\ \vdots \\ \vec{P_{\text{out}}}(t-\tau_n) \end{pmatrix}. \quad (13)$$

W_k describes a sparse matrix of weights associated with the delay in element k of the unique delay vector U. To simulate various system configurations, we used Runge–Kutta methods iteratively within a standard DDE solver in MATLAB. This formulation allows the simulation of arbitrary networks of excitable lasers.

Since weighing and delaying are both linear operations, they can be implemented optically with passive devices. A physical architecture of a tunable weight-delay network is illustrated in Fig. 9. Excitable lasers send pulses into an optical network, which may use amplifiers, filters, or switching technologies to sort and distribute the spikes en route to other excitable lasers. The combined inputs incident on a single laser embedded within the network are then weighted and delayed individually by tunable optical attenuators and delay lines before arrival.

A tunable weight-delay input array as depicted in Fig. 9—which can be thought of as the photonic equivalent of a dendritic tree—has been experimentally realized in a photonic beam former [47]. With the appropriate integrated, tunable attenuators and delay lines—which can be implemented using ring resonators structures [48], [49] or other technologies [50], [51]—this array could be compacted into a small footprint, allowing for massive network integration. Further work will explore the scalability of this approach. Described next are several circuits that could potentially utilize this architecture to perform tasks specific to spike processing.

[4]We absorb the attenuation or amplification the pulse experiences en route to its destination along with the responsivity of the perturbation to the incident pulse into a single weight parameter W_{ij}.

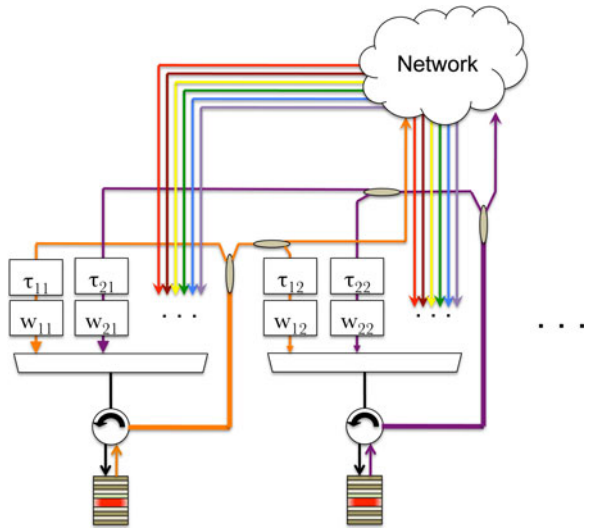

Fig. 9. A physical architecture of a photonic neural network with tunable weights and delays (two lasers displayed). Laser outputs are separated from inputs with use of a circulator and travel into an optical network that evenly distributes spiking signals across the entire device landscape. Before signals arrive at their respective destinations, they interface with a front-end control unit that applies weights w_{ij} and delays τ_{ij} to signals traveling from lasers i to j.

A. *Multistable System*

Multistability represents a crucial property of dynamical systems and arises out of the formation of hysteric attractors. This phenomenon plays an important role in the formation of memory in processing systems. Here, we describe a network of two interconnected excitable lasers, each with two incoming connections and identical weights and delays, as illustrated in Fig. 10(a). The system is recursive rather than feedforward, possessing a network path that contains a closed loop. This allows the system to exhibit hysteresis.

Results for the two laser multistable system are shown in Fig. 10(b). The network is composed of two lasers, interconnected via optical connections with a delay of 1 ns. An excitatory pulse travels to the first unit at $t = 5$ ns, initiating the system to settle to a new attractor. The units fire pulses repetitively at fixed intervals before being deactivated by a precisely timed inhibitory pulse at $t = 24$ ns. It is worth noting that the system is also capable of stabilizing to other states, including those with multiple pulses or different pulse intervals. It, therefore, acts as a kind of optical pattern buffer over longer time scales. Ultimately, this circuit represents a test of the network's ability to handle recursive feedback. In addition, the stability of the system implies that a network is cascadable since a self-referent connection is isomorphic to an infinite chain of identical lasers with identical weights W between every node. Because this system successfully maintains the stability of self-pulsations, processing

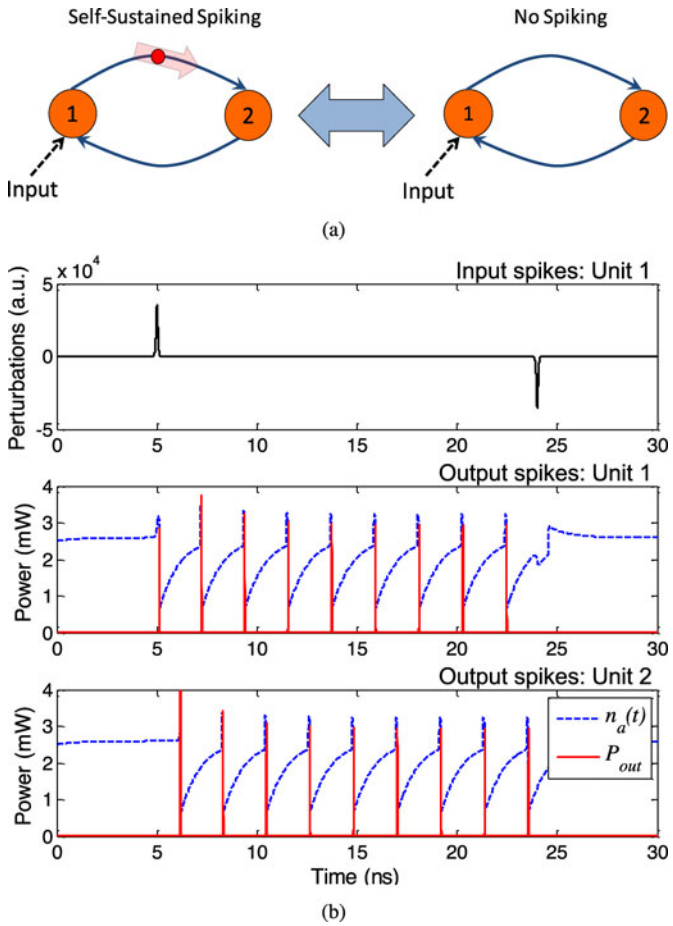

Fig. 10. (a) Bistability schematic—In this configuration, two lasers are connected symmetrically to each other. (b) A simulation of a two laser system exhibiting bistability with connection delays of 1 ns. The input perturbations to unit 1 are plotted, followed by the output powers of units 1 and 2, which include scaled version of the carrier concentrations of their gain sections as the dotted blue lines. Excitatory pulses are represented by positive perturbations while inhibitory pulses are represented by negative perturbations. An excitatory input excites the first unit, causing a pulse to be passed back and forth between the nodes. A precisely timed inhibitory pulse terminates the sequence.

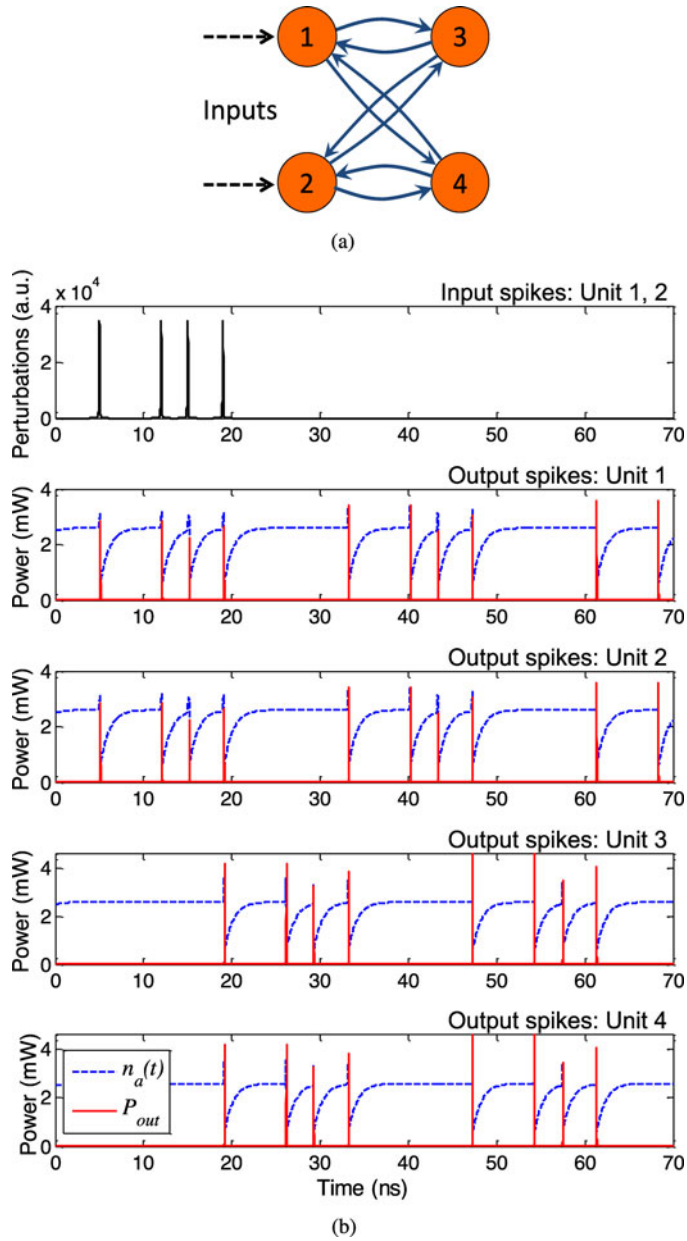

Fig. 11. (a) Synfire schematic—In this configuration, two groups of lasers are connected symmetrically two each other. (b) Simulation of a four laser circuit forming synfire chains with connection delays of 14 ns. The input perturbations to units 1, 2 are plotted over time, followed by the output powers of units 1–4 with the scaled carrier concentrations of their gain sections as the dotted blue lines. A characteristic spike pattern is repeatedly passed back and forth between the left and right set of nodes.

networks of excitable VCSELs are theoretically capable of cascadibility and information retention during computations.

B. *Synfire Chain*

Synfire chains have been proposed by Abeles [52] as a model of cortical function. A synfire chain is essentially a feedforward network of neurons with many layers (or pools). Each neuron in one pool feeds many excitatory connections to neurons in the next pool, and each neuron in the receiving pool is excited by many neurons in the previous pool, so that a wave of activity can propagate from pool to pool in the chain. It has been postulated that such a wave corresponds to an elementary cognitive event [53].

Synfire chains can use *population encoding* to reduce jitter accumulation when sending, receiving, or storing a spatiotemporal bit pattern of spikes [41]. Population encoding works by making multiple copies of a pulse and distributing it via several distinct channels. When these copies arrive and recombine onto the same subsequent processing unit, jitter and amplitude noise accumulated in statistically uncorrelated channels are averaged and therefore reduced. One of the key features of a hybrid analog-digital system such as an spiking neural networks (SNN) is that many analog nodes can process in a distributed and redundant way to reduce noise accumulation. Recruiting a higher number of neurons to accomplish the same computation is an effective and simple way of reducing spike error rates.

Fig. 11(a) shows a demonstration of a simple four-laser synfire chain with feedback connections. The chain is simply a two

unit expansion of each node in the multistability circuit from Fig. 10(a). Like the multistability circuit, recursion allows the synfire chain to possess hysteric properties; however, the use of two lasers for each logical node provides processing redundancy and increases reliability. Once the spike pattern is input into the system as excitatory inputs injected simultaneously into the first two lasers, it is continuously passed back and forth between each set of two nodes. The spatiotemporal bit pattern persists after several iterations and is thereby stored in the network as depicted in Fig. 11(b).

C. Spatiotemporal Pattern Recognition Circuit

The concept of polychrony, proposed by Izhikevich [42] is defined as an event relationship that is precisely time-locked to firing patterns but not necessarily synchronous. Polychronization presents a minimal spiking network that consists of cortical spiking neurons with axonal delays and synaptic time dependent plasticity (STDP), an important learning rule for spike-encoded neurons. As a result of the interplay between the delays and STDP, spiking neurons spontaneously self-organize into groups and generate patterns of stereotypical polychronous activity.

One of the key properties of polychronization is the ability to perform *delay logic* to perform spatiotemporal pattern recognition. As shown in Fig. 12(a), we construct a simple three unit pattern recognition circuit of excitable lasers with carefully tuned delay lines, where each subsequent neuron in the chain requires stronger perturbations to fire. The resulting simulation is shown in Fig. 12(b). Three excitatory inputs separated sequentially by $\Delta t_1 = 5$ ns and $\Delta t_2 = 10$ ns are incident on all three units. The third is configured only to fire if it receives an input pulse and pulses from the other two simultaneously. The system, therefore, only reacts to a specific spatiotemporal bit pattern.

Although this circuit is simple, the ability to perform temporal logic implies that excitable, neuromorphic systems are capable of categorization and decision making. Two existing applications utilize temporal logic, including light detection and ranging sensitivity that is analogous to an owl's echolocation system and the escape response of a crayfish [54], [55]. Combined with learning algorithms such as STDP which has recently been demonstrated in optics [56], networks could potentially perform more complex tasks such as spike-pattern cluster analysis.

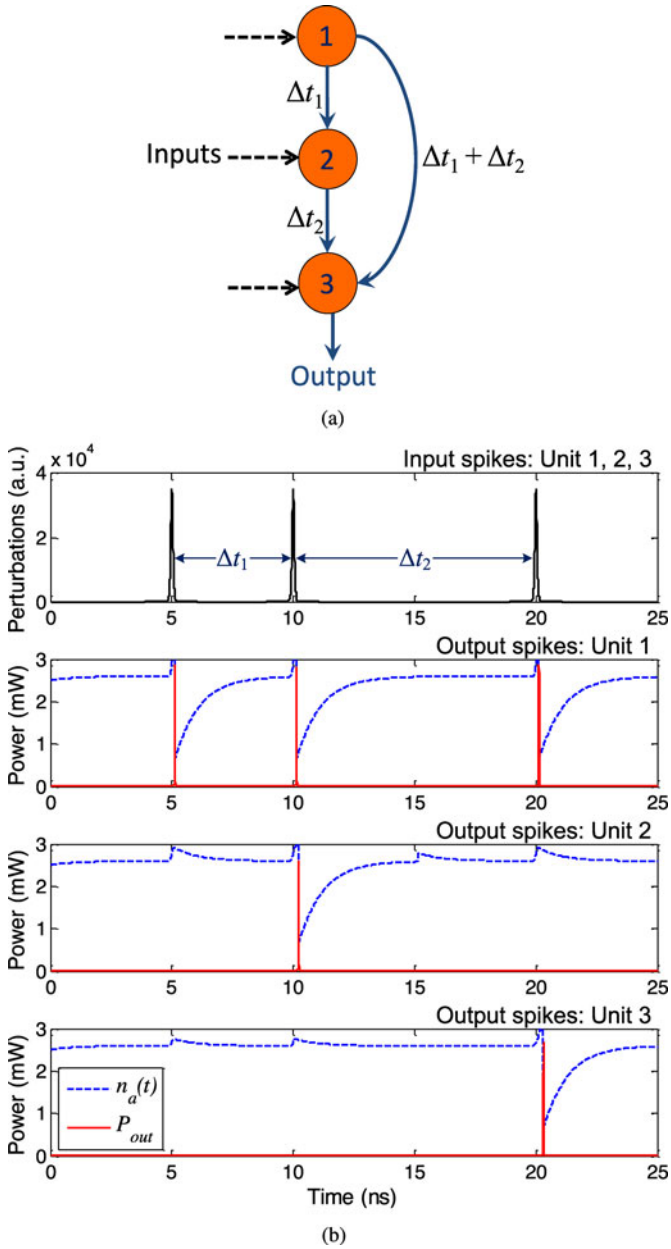

Fig. 12. (a) Schematic of a three-laser circuit that can recognize specific spatiotemporal bit patterns. (b) A simulation of a spatiotemporal recognition circuit with $\triangle t_1 = 5$ ns and $\triangle t_2 = 10$ ns. The input perturbation to unit 1 is plotted, along with the output powers of units 1–3 with the scaled carrier concentrations of their gain sections as the dotted blue lines. The third neuron fires during the triplet spike pattern with time delays $\triangle t_1$ and $\triangle t_2$ between spikes.

V. Discussion

A. Comparing Technological Platforms

Cortically-inspired microelectronic architectures have traditionally targeted biological time scales. Several proposals [3], [57] suggest using a crossbar array to network neurons together, essentially a dense mesh of wires overlaying the CMOS (processor) substrate. This is to achieve a massive fan-in and fan-out per connection, which is typical in neural networks but less critical in conventional processors. Several popular approaches aim to achieve clock rates comparable to biological time scales, but transmitting high-bandwidth spikes at the speeds of current processors (gigahertz)—which tend to have high bandwidth requirements—could overrun the system with electromagnetic interference (EMI). Signals would quickly attenuate, disperse, or couple together unfavorably, especially on a crossbar array, which has a large area of closely packed signal wires. In contrast, light can support the high frequency components of spikes and large fan-in and fan-out per connection with almost no crosstalk through techniques such as wavelength division multiplexing. Achieving both high speeds and large interconnection densities simultaneously is comparably impossible in electronics.

The ability to make a technology that complements the physical constraints that guide it, rather than abstracting them away entirely, represents an important step in streamlining efficiency and performance. Optics is a perfect fit for high bandwidth spike information and could represent a highly efficient processing scheme that ties closely to its underlying physics.

B. Improvements Over Previous Models

Past photonic neurons have demonstrated important features of biological neurons but did not integrate enough properties together to make effective processors. One of the first implementations of a photonic spiking neuron [15] achieved noise suppression and thresholding through a nonlinear optical loop mirror, generated pulses synchronously via a mode-locked laser, and utilized an SOA for integration. This model demonstrated temporal integration and spike thresholding, but too much excitation could lead to the release of multiple pulses, degrading spike-encoded information. In addition, spikes were not asynchronous, making the output of the system digital.

The fully functioning photonic neuron demonstrated by Kravstsov [16] integrated both excitation and inhibition, but also suffered from the problems mentioned previously. A newer asynchronous model was proposed in [17] that generated spikes based on incoming spikes. Although the system could emit a pulse at analog times, because the system did not generate its own spikes through internal mechanisms, the spikes could eventually degrade into noise as nonspike inputs led to nonspike outputs.

The excitable models are a step in the right direction, given the similarities between lasers and biological phenomena and the stability of feedback systems. However, both of the recent proposals [22], [24] have a large, base intensity level that underlies spike outputs. Spikes resemble variations of the output intensity rather than pulses. A base-level intensity can potentially be debilitating: by adding constant optical power into the inputs, one can change the equilibrium levels of internal state variables. Programming the synaptic weights w_{ij} would simultaneously modulate the internal dynamics of each laser in addition to the strength between connections, causing forward propagating system dependences. In addition, a constant base level intensity could increase amplified spontaneous emission noise within the network, decreasing its robustness.

Although biological neurons also have a continuously varying state variable (voltage) during an an action potential, the actual response is thresholded by voltage-gated reversal potentials that only induce neurotransmitter release between cells during a spike. It is unclear if the semispiking signals emitted by these other lasers could be processed effectively by subsequent units in a network. These lasers would probably require an optical thresholder such as [58] or a nonlinear OEO (optical–electrical–optical) connection in addition to the units already proposed to work effectively.

The neuron model described here avoids many previous issues by combining an excitable approach with some of the ideas of the feedforward model. The integration of a laser gain section—which is dynamically analogous to an SOA—and a saturable absorber, which is essentially a feedback version of the thresholder used in the fiber model, leads to many desirable properties and a close analogy with biology, including the formation of highly stereotyped and well-defined optical spikes.

VI. Conclusion

In summary, we have proposed and simulated a novel optical signal processing device that is capable of implementing cortical-inspired algorithms. We have shown that, unlike previous models, our device can effectively perform cognitive algorithms at ultrafast time scales. This model is demonstrably analogous to an LIF neuron, and networks of such devices are stable, robust to noise, and can recognize patterns.

Spike processing algorithms are well understood in a number of important biological sensory processing systems and are finding growing use in signal processing applications [27]. The combination of these physiological principles with engineering not only helps in studying biological neural circuits [59], but the pairing of computational technology with underlying physics could achieve new domains of application and study.

Ultrafast optical STDP, one of the most important algorithms for spike-based learning, has recently been demonstrated experimentally [56]. All the components used in this experiment—including the Mach–Zehnder configuration, the EAM, and the SOA—can be fabricated with a small footprint in planar photonics. Integrating this together with LIF excitable neurons on a single chip could lead to systems that emulate a well-established paradigm for adaptive computing on a scalable platform. These compact, adaptive, and unconventional processing systems would operate on unprecedented time scales. Large networks could potentially be constructed as liquid state machines for optical reservoir computing [60] to aid in the study of biology or open up new ultrafast environments such as the RF spectrum for neuromorphic experimentation.

Acknowledgment

The author would like to acknowledge D. Rosenbluth at the Lockheed Martin Advanced Technology Laboratory for fruitful discussions and would also like to acknowledge Prof. M. Fok at the University of Georgia for guidance, suggestions, and support.

References

[1] P. Merolla, J. Arthur, F. Akopyan, N. Imam, R. Manohar, and D. Modha, "A digital neurosynaptic core using embedded crossbar memory with 45 pJ per spike in 45 nm," in *Proc. IEEE Custom Integr. Circuits Conf.*, Piscataway, NJ, USA, 2011, pp. 1–4.

[2] J. Seo, B. Brezzo, Y. Liu, B. Parker, S. Esser, R. Montoye, B. Rajendran, J. Tierno, L. Chang, D. Modha, and D. J. Friedman, "A 45 nm CMOS neuromorphic chip with a scalable architecture for learning in networks of spiking neurons," in *Proc. Custom Integr. Circuits Conf.*, Piscataway, NJ, USA, 2011, pp. 1–4

[3] G. Snider, "Self-organized computation with unreliable, memristive nanodevices," *Nanotechnology*, vol. 18, no. 36, p. 365202, 2007

[4] K. Boahen, "Communicating neuronal ensembles between neuromorphic chips," *Neuromorph. Syst. Eng.*, vol. 447, pp. 229–259, 1998.

[5] J. Han and P. Jonker, "A defect-and fault-tolerant architecture for nanocomputers," *Nanotechnology*, vol. 14, no. 2, pp. 224–230, 2003.

[6] N. Mathur, "Beyond the silicon roadmap," *Nature*, vol. 419, no. 6907, pp. 573–575, 2002.

[7] A. G. Andreou, K. A. Boahen, P. O. Pouliquen, A. Pavasovic, R. E. Jenkins, and K. Strohbehn, "Current-mode subthreshold MOS circuits for analog VLSI neural systems," *IEEE Trans. Neural Netw.*, vol. 2, no. 2, pp. 205–213, Mar. 1991.

[8] D. S. Modha, R. Ananthanarayanan, S. K. Esser, A. Ndirango, A. J. Sherbondy, and R. Singh, "Cognitive computing," *Commun. ACM*, vol. 54, no. 8, pp. 62–71, Aug. 2011.

[9] G. Snider, R. Amerson, D. Carter, H. Abdalla, M. S. Qureshi, J. Léveillé, M. Versace, H. Ames, S. Patrick, B. Chandler, A. Gorchetchnikov, and E. Mingolla, "From synapses to circuitry: Using memristive memory to explore the electronic brain," *Computer*, vol. 44, no. 2, pp. 21–28, 2011.

[10] S. Thorpe, A. Delorme, and R. Van Rullen, "Spike-based strategies for rapid processing," *Neural Netw.*, vol. 14, no. 6–7, pp. 715–725, 2001.

[11] M. Sushchik Jr., N. Rulkov, L. Larson, L. Tsimrin, H. Abarbanel, K. Yao, and A. Volkovskii, "Chaotic pulse position modulation: A robust method of communicating with chaos," *IEEE Commun. Lett.*, vol. 4, no. 4, pp. 128–130, Apr. 2000.

[12] D.-S. Shiu and J. M. Kahn, "Differential pulse-position modulation for power-efficient optical communication," *IEEE Trans. Commun.*, vol. 47, no. 8, pp. 1201–1210, 1999.

[13] R. Sarpeshkar, "Analog versus digital: Extrapolating from electronics to neurobiology," *Neural Comput.*, vol. 10, no. 7, pp. 1601–1638, Oct. 1998.

[14] K. Boahen, "Neurogrid: Emulating a million neurons in the cortex," in *Proc. IEEE Int. Conf. Eng. Med. Biol. Soc.*, 2006, p. 6702.

[15] D. Rosenbluth, K. Kravtsov, M. P. Fok, and P. R. Prucnal, "A high performance photonic pulse processing device," *Opt. Exp.*, vol. 17, no. 25, pp. 22 767–22 772, Dec. 2009.

[16] K. Kravtsov, M. P. Fok, D. Rosenbluth, and P. R. Prucnal, "Ultrafast all-optical implementation of a leaky integrate-and-fire neuron," *Opt. Exp.*, vol. 19, no. 3, pp. 2133–2147, Jan. 2011.

[17] M. P. Fok, Y. Tian, D. Rosenbluth, and P. R. Prucnal, "Asynchronous spiking photonic neuron for lightwave neuromorphic signal processing," *Opt. Lett.*, vol. 37, no. 16, pp. 3309–3311, Aug. 2012.

[18] M. Giudici, C. Green, G. Giacomelli, U. Nespolo, and J. R. Tredicce, "Andronov bifurcation and excitability in semiconductor lasers with optical feedback," *Phys. Rev. E*, vol. 55, no. 6, pp. 6414–6418, Jun. 1997.

[19] V. Z. Tronciu, H. J. Wunsche, M. Radziunas, and K. R. Schneider, "Excitability of lasers with integrated dispersive reflector," *Proc. SPIE*, vol. 4283, pp. 347–354, Jul. 2001.

[20] B. Krauskopf, K. Schneider, J. Sieber, S. Wieczorek, and M. Wolfrum, "Excitability and self-pulsations near homoclinic bifurcations in semiconductor laser systems," *Opt. Commun.*, vol. 215, no. 4–6, pp. 367–379, Jan. 2003.

[21] E. Izhikevich, *Dynamical Systems in Neuroscience: The Geometry of Excitability and Bursting*. Cambridge, MA, USA: MIT press, 2006.

[22] W. Coomans, L. Gelens, S. Beri, J. Danckaert, and G. Van der Sande, "Solitary and coupled semiconductor ring lasers as optical spiking neurons," *Phys. Rev. E*, vol. 84, no. 3, pp. 036209-1–036209-8, 2011.

[23] W. Coomans, L. Gelens, L. Mashal, S. Beri, G. Van der Sande, J. Danckaert, and G. Verschaffelt, "Semiconductor ring lasers as optical neurons," in *Proc. International Society for Optics and Photonics.*, Bellingham, WA, USA, 2012, pp. 84 321I–84 321I.

[24] A. Hurtado, K. Schires, I. Henning, and M. Adams, "Investigation of vertical cavity surface emitting laser dynamics for neuromorphic photonic systems," *Appl. Phys. Lett.*, vol. 100, no. 10, pp. 103 703–103 703, 2012.

[25] E. Izhikevich, "Which model to use for cortical spiking neurons?," *IEEE Trans. Neural Netw.*, vol. 15, no. 5, pp. 1063–1070, Sep. 2004.

[26] C. Koch, *Biophysics of Computation: Information Processing in Single Neurons (Computational Neuroscience)*. Oxford, U.K.: Oxford Univ. Press, 1998.

[27] W. Maass and C. M. Bishop, Eds., *Pulsed Neural Networks*. Cambridge, MA, USA: MIT Press, 1999.

[28] G. Spühler, R. Paschotta, R. Fluck, B. Braun, M. Moser, G. Zhang, E. Gini, and U. Keller, "Experimentally confirmed design guidelines for passively q-switched microchip lasers using semiconductor saturable absorbers," *JOSA B*, vol. 16, no. 3, pp. 376–388, 1999.

[29] H. Wenzel, U. Bandelow, H. Wunsche, and J. Rehberg, "Mechanisms of fast self pulsations in two-section dfb lasers," *IEEE J. Quantum Electron.*, vol. 32, no. 1, pp. 69–78, Jan. 1996.

[30] D. Nugent, R. Plumb, M. Fisher, and D. Davies, "Self-pulsations in vertical-cavity surface emitting lasers," *Electron. Lett.*, vol. 31, no. 1, pp. 43–44, 1995.

[31] J. Dubbeldam and B. Krauskopf, "Self-pulsations of lasers with saturable absorber: Dynamics and bifurcations," *Opt. Commun.*, vol. 159, no. 4, pp. 325–338, 1999.

[32] F. Koyama, "Recent advances of vcsel photonics," *J. Lightw. Technol.*, vol. 24, no. 12, pp. 4502–4513, 2006.

[33] S. Barbay, R. Kuszelewicz, and A. M. Yacomotti, "Excitability in a semiconductor laser with saturable absorber," *Opt. Lett.*, vol. 36, no. 23, pp. 4476–4478, Dec. 2011.

[34] Y. Li, T. Wang, and R. Linke, "VCSEL-array-based angle-multiplexed optoelectronic crossbar interconnects," *Appl. Opt.*, vol. 35, no. 8, pp. 1282–1295, 1996.

[35] D. Taillaert, W. Bogaerts, P. Bienstman, T. Krauss, P. Van Daele, I. Moerman, S. Verstuyft, K. De Mesel, and R. Baets, "An out-of-plane grating coupler for efficient butt-coupling between compact planar waveguides and single-mode fibers," *IEEE J. Quantum Electron.*, vol. 38, no. 7, pp. 949–955, Jul. 2002.

[36] D. Louderback, G. Pickrell, H. Lin, M. Fish, J. Hindi, and P. Guilfoyle, "VCSELS with monolithic coupling to internal horizontal waveguides using integrated diffraction gratings," *Electron. Lett.*, vol. 40, no. 17, pp. 1064–1065, 2004.

[37] L. Coldren, S. Corzine, and M. Mashanovitch, *Diode Lasers and Photonic Integrated Circuits*, (Series Wiley Series in Microwave and Optical Engineering). New York, NY, USA: Wiley, 2011.

[38] B. J. Shastri, C. Chen, K. D. Choquette, and D. V. Plant, "Circuit modeling of carrier–photon dynamics in composite-resonator vertical-cavity lasers," *IEEE J. Quantum Electron.*, vol. 47, no. 12, pp. 1537–1546, Dec. 2011.

[39] D. Nugent, R. Plumb, M. Fisher, and D. Davies, "Self-pulsations in vertical-cavity surface emitting lasers," *Electron. Lett.*, vol. 31, no. 1, pp. 43–44, Jan. 1995.

[40] G. E. Giudice, D. V. Kuksenkov, H. Temkin, and K. L. Lear, "Differential carrier lifetime in oxide-confined vertical cavity lasers obtained from electrical impedance measurements," *Appl. Phys. Lett.*, vol. 74, no. 7, pp. 899–901, 1999.

[41] M. Herrmann, J. A. Hertz, and A. Prugel-Bennett, "Analysis of synfire chains," *Netw.: Comput. Neural Syst.*, vol. 6, no. 3, pp. 403–414, 1995.

[42] E. M. Izhikevich, "Polychronization: Computation with spikes," *Neural Comput.*, vol. 18, no. 2, pp. 245–282, Feb. 2006.

[43] C. Eliasmith, "A unified approach to building and controlling spiking attractor networks," *Neural Comput.*, vol. 17, no. 6, pp. 1276–1314, 2005.

[44] Y. Ikegaya, G. Aaron, R. Cossart, D. Aronov, I. Lampl, D. Ferster, and R. Yuste, "Synfire chains and cortical songs: Temporal modules of cortical activity," *Sci. Signall.*, vol. 304, no. 5670, pp. 559–564, 2004.

[45] B. Szatmáry and E. M. Izhikevich, "Spike-timing theory of working memory," *PLoS Comput. Biol.*, vol. 6, no. 8, p. e1000879, 2010.

[46] Y. Tian, M. Fok, and P. Prucnal, "Experimental characterization of simultaneous gain pumping and depletion in a semiconductor optical amplifier," in *Proc. IEEE Lasers Electro-Opt. Conf.*, Piscataway, NJ, USA, 2011, pp. 1–2.

[47] J. Chang, M. P. Fok, R. M. Corey, J. Meister, and P. R. Prucnal, "Highly scalable adaptive photonic beamformer using a single mode to multimode optical combiner," *IEEE Microw. Wireless Compon. Lett.*, to be published

[48] F. Xia, L. Sekaric, and Y. Vlasov, "Ultracompact optical buffers on a silicon chip," *Nature Photon.*, vol. 1, no. 1, pp. 65–71, 2006.

[49] Q. Xu, B. Schmidt, S. Pradhan, and M. Lipson, "Micrometre-scale silicon electro-optic modulator," *Nature*, vol. 435, no. 7040, pp. 325–327, 2005.

[50] C. J. Chang-Hasnain, P.-C. Ku, J. Kim, and S.-L. Chuang, "Variable optical buffer using slow light in semiconductor nanostructures," *Proc. IEEE*, vol. 91, no. 11, pp. 1884–1897, Nov. 2003.

[51] W. M. Green, M. J. Rooks, L. Sekaric, and Y. A. Vlasov, "Ultra-compact, low RF power, 10 gb/s silicon mach-zehnder modulator," *Opt. Exp.*, vol. 15, no. 25, pp. 17 106–17 113, 2007.

[52] M. Abeles, *Corticonics: Neural Circuits of the Cerebral Cortex*. Cambridge, England: Cambridge Univ. Press, 1991.

[53] E. Bienenstock, "A model of neocortex," *Netw.: Comput. Neural Syst.*, vol. 6, no. 2, pp. 179–224, 1995.

[54] M. P. Fok, H. Deming, M. Nahmias, N. Rafidi, D. Rosenbluth, A. Tait, Y. Tian, and P. R. Prucnal, "Signal feature recognition based on lightwave neuromorphic signal processing," *Opt. Lett.*, vol. 36, no. 1, pp. 19–21, Jan. 2011.

[55] P. R. Prucnal, M. P. Fok, D. Rosenbluth, and K. Kravtsov, "Lightwave neuromorphic signal processing," in *Proc. Int. Conf. Inf. Photon.*, May 2011, pp. 1–2.

[56] M. P. Fok, Y. Tian, D. Rosenbluth, and P. R. Prucnal, "Pulse lead/lag timing detection for adaptive feedback and control based on optical spike timing dependent plasticity," *Opt. Lett.*, vol. 38, no. 4, pp. 419–421, 2013.

[57] K. Likharev, A. Mayr, I. Muckra, and Ö. Türel, "Crossnets: High-performance neuromorphic architectures for cmol circuits," *Ann. New York Acad. Sci.*, vol. 1006, no. 1, pp. 146–163, 2003.

[58] A. N. Tait, B. J. Shastri, M. P. Fok, M. A. Nahmias, and P. R. Prucnal, "The dream: An integrated photonic thresholder," *J. Lightw. Technol.*, vol. 31, no. 8, pp. 1263–1272, Apr. 2013.
[59] L. S. Smith and A. Hamilton, *Neuromorphic Systems: Engineering Silicon From Neurobiology*. Singapore: World Scientific Publishing Company Incorporated, 1998, vol. 10.
[60] K. Vandoorne, W. Dierckx, B. Schrauwen, D. Verstraeten, R. Baets, P. Bienstman, and J. V. Campenhout, "Toward optical signal processing using photonic reservoir computing," *Opt. Exp.*, vol. 16, no. 15, pp. 11 182–11 192, Jul. 2008.

Mitchell A. Nahmias (S'11) received the B.Sci.Eng. (Hons.) in electrical engineering from Princeton University, Princeton, NJ, USA, in 2012, where he is currently working toward the Ph.D. degree in electrical engineering in the Lightwave Communications Group, Department of Electrical Engineering.

He was an undergraduate Researcher for the summers of 2011–2012 at the MIRTHE Center, Princeton University. His research interests include laser dynamics for processing, bio-inspired engineering, and nontraditional computing architectures.

Mr. Nahmias received the John Ogden Bigelow Jr. Prize in Electrical Engineering and was was the co-winner of the Best Engineering Physics Independent Work Award for his senior thesis. He is also a Student Member of the Optical Society of America. He is a recipient of the National Science Foundation Graduate Research Fellowship.

Bhavin J. Shastri (S'03–M'11) received the B.Eng. (with distinction, Hons.), M.Eng., and Ph.D. degrees in electrical engineering, all from McGill University, Montreal, QC, Canada, in 2005, 2007, and 2011, respectively.

He is currently a Postdoctoral Research Fellow at the Lightwave Communications Laboratory, Princeton University, Princeton, NJ, USA. His research interests include ultrafast cognitive computing—neuromorphic engineering with photonic neurons, high-speed burst-mode clock and data recovery circuits, optoelectronic-VLSI systems, optical access networks, machine learning, and computer vision.

Dr. Shastri received the following research awards: 2012 D. W. Ambridge Prize for the top graduating Ph.D. student, nomination for the 2012 Canadian Governor General Gold Medal, IEEE Photonics Society 2011 Graduate Student Fellowship, 2011 Postdoctoral Fellowship from National Sciences and Engineering Research Council of Canada (NSERC), 2011 SPIE Scholarship in Optics and Photonics, a Lorne Trottier Engineering Graduate Fellow, and a 2008 Alexander Graham Bell Canada Graduate Scholarship from NSERC. He also received the Best Student Paper Awards at the 2010 IEEE Midwest Symposium on Circuits and Systems, the co-recipient of the Silver Leaf Certificate at the 2008 IEEE Microsystems and Nanoelectronics Conference, the 2004 IEEE Computer Society Lance Stafford Larson Outstanding Student Award, and the 2003 IEEE Canada Life Member Award. He was the President/Cofounder of the McGill OSA Student Chapter.

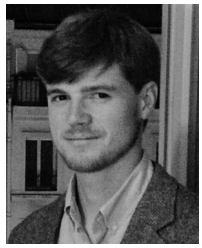

Alexander N. Tait (S'11) received the B.Sci.Eng. (Hons.) in electrical engineering from Princeton University, Princeton, NJ, USA, in 2012, where he is currently working toward the Ph.D. degree in electrical engineering in the Lightwave Communications Group, Department of Electrical Engineering.

He was a research intern for the summers of 2008–2010 at the Laboratory for Laser Energetics, University of Rochester, Rochester, NY, USA, and an Undergraduate Researcher for the summers of 2011–2012 at the MIRTHE Center, Princeton University, Princeton, NJ, USA. His research interests include photonic devices for nonlinear signal processing, integrated systems, neuromorphic engineering, and hybrid analog-digital signal processing and computing.

Mr. Tait is a Student Member of the Optical Society of America. He is a recipient of the National Science Foundation Graduate Research Fellowship. He is a co-recipient of the Optical Engineering Award of Excellence from the Department of Electrical Engineering at Princeton. He has co-authored three journal papers appearing in *Optics Letters*, *the Journal of Applied Physics*, and *the International Journal of Hydrogen Energy*.

Paul R. Prucnal (S'75–M'79–SM'90–F'92) received the A.B. degree from Bowdoin College (summa cum laude) in math and physics (Highest Hons.), where he was elected to Phi Beta Kappa. He then received the M.S., M.Phil., and Ph.D. degrees from Columbia University, New York, NY, USA, where he was elected to the Sigma Xi honor society.

He is currently a Professor of electrical engineering at Princeton University, where he has also served as the Founding Director of the Center for Photonics and Optoelectronic Materials, and is currently the Director of the Center for Network Science and Applications. He has held visiting faculty positions at the University of Tokyo and University of Parma.

Prof. Prucnal was an Area Editor of the IEEE TRANSACTIONS ON COMMUNICATIONS for optical networks, and was the Technical Chair and General Chair of the IEEE Topical Meeting on Photonics in Switching in 1997 and 1999, respectively. He is a Fellow of the OSA, and a recipient of the Rudolf Kingslake Medal from the SPIE, cited for his seminal paper on photonic switching. In 2006, he was awarded the Gold Medal from the Faculty of Physics, Mathematics, and Optics from Comenius University in Slovakia, for his contributions to research in photonics. He has received Princeton Engineering Council Awards for Excellence in Teaching, the University Graduate Mentoring Award, and the Walter Curtis Johnson Prize for Teaching Excellence in electrical engineering, as well as the Distinguished Teacher Award from Princetons School of Engineering and Applied Science. He is editor of the book *Optical Code Division Multiple Access*: *Fundamentals and Applications.*